www.czasopisma.pan.pl PAN POLSKA AKADEMIA NAUK www.journals.pan.pl

Arch. Metall. Mater. **66** (2021), 1, 145-152

DOI: 10.24425/amm.2021.134770

YIMING LI[1], XIAOMIN HUANG[1,2*], HONGCHAO JI[1,2,3*], YAOGANG LI[1],
BAOYU WANG[2], XUEFENG TANG[4]

STUDY ON DYNAMIC RECRYSTALLIZATION MODELS OF 21-4N HEAT RESISTANT STEEL

The high-temperature deformation process and dynamic recrystallization (DRX) process of 21-4N were investigated under the conditions of the deformation temperature range of 1273~1453K, the strain rate range of 0.01~10s^{-1} and the deformation degree of 60% (the total deformation is 0.916) by using Gleeble-1500D thermal simulated test machine. The curves of stress-strain ($\sigma - \varepsilon$) were obtained, and the curves of work hardening rate (θ) and strain (ε) were obtained by taking derivative of $\sigma - \varepsilon$. The DRX critical strains under different conditions were determined by the curves of work hardening rate ($\theta - \varepsilon$), and the DRX critical strain model was established. The peak strains of 21-4N were obtained by the curves of $\sigma - \varepsilon$, the relationship between peak stress (σ_p) and critical strain (ε_c) was determined, and the peak strain model was established. The DRX volume fraction models of 21-4N were established by using Avrami equation. The DRX grain size of 21-4N was calculated by Image Pro Plus 6.0, and its DRX grain size models were established.

Keywords: 21-4N, hot deformation, dynamic recrystallization, critical strain, volume fraction

1. Introduction

21-4N is a heat-resistant steel that can be strengthened by heat treatment. It is characterized by good oxidation resistance, high temperature mechanical properties and chemical stability and so on. It is widely used in extreme environments such as high temperature, high pressure, corrosion and so on. And it is a preferred material of choice for the manufacture of various engine valves [1-2].

During the hot deformation of metals and alloys, DRX plays an important role on the microstructure evolution. It can soften the deformation-hardened metals and alloys, repair its plasticity and ductility, and improve the plasticity. It can also refine grains and control the microstructure of the final forging [3]. The Alloys based on Cu, Fe, Al and Ni do not undergo phase transformation during hot deformation. Therefore, DRX is the only way to control the grain size, morphology and microstructure of such alloy forgings [4].

In recent years, many scholars have conducted lots of researches on DRX models of different metals. Wang et al. [5] studied the high-temperature deformation process of 316LN. The DRX mathematical model of 316LN was established and its DRX softening mechanism was determined. Favre et al. [6] combined the average field model with reverse engineering method to study the microstructure evolution of L-605 cobalt alloy during hot deformation, and its DRX kinetics model was established. Fang et al. [7] studied the DRX process of FGH96, the DRX models of double-pass were established. The influence of deformation conditions (deformation temperature and strain rate) on DRX was determined, the difference between the first pass and the second pass model was analyzed. Liu et al. [8] proposed a new three-stage DRX model to describe the DRX process, and the most suitable range of strain for DRX was determined. Jiang et al. [9] studied the DRX process and microstructure evolution of 690 alloy, the DRX model and grain growth model were established, and the accuracy of models by finite element analysis were verified. Ji et al. [10] studied the high-temperature deformation process and DRX process of Cu-0.4Mg alloy. The work hardening rate was calculated and its DRX kinetics model was established by using $\sigma - \varepsilon$ data. Xu et al. [11] studied the DRX process of AZ61 and established its DRX mechanics model. Thomas et al. [12] studied the DRX process of martensitic steel, the structural evolution models was established, the high correlation between the initial microstructure of martensitic steel and DRX kinetics was deter-

[1] NORTH CHINA UNIVERSITY OF SCIENCE AND TECHNOLOGY, COLLEGE OF MECHANICAL ENGINEERING, HEBEI TANGSHAN, 063210, CHINA
[2] UNIVERSITY OF SCIENCE AND TECHNOLOGY, BEIJING SCHOOL OF MECHANICAL ENGINEERING, BEIJING 100083, CHINA
[3] UNIVERSITY OF SCIENCE AND TECHNOLOGY BEIJING, NATIONAL CENTER FOR MATERIALS SERVICE SAFETY, BEIJING 100083, CHINA
[4] THE HONG KONG POLYTECHNIC UNIVERSITY, DEPARTMENT OF MECHANICAL ENGINEERING, HUNG HOM, KOWLOON, HONG KONG, CHINA

* Corresponding authors: hxm8606@126.com; jihongchao@ncst.edu.com

mined. Chen et al. [13] studied the DRX process of 42CrMo steel by thermal compression test and established the DRX mechanics model, the influence of deformation conditions and the original grain size on the DRX process of 42CrMo was analyzed. At present, most studies on DRX models focus on magnesium alloys, aluminum alloys and other alloys, but few studies focus on 21-4N heat-resistant steel. Therefore, it is necessary to conduct a detailed study on the DRX model of 21-4N heat-resistant steel.

Based on the isothermal thermal compression test of 21-4N, this study analyzed the influence rule of deformation conditions on the $\sigma - \varepsilon$ curves, conducted the relationship between θ and ε by using $\sigma - \varepsilon$ curves, established the DRX critical strain and peak strain model, volume fraction models and grain size models and the accuracy of four models were verified.

2. Materials and Experimental

The material in this study is 21-4N and its composition is shown in Table 1.

TABLE 1

The composition of the 21-4N (wt.%)

Cr	Mn	Ni	C	N	Si	P	S	Fe
20-22	8-10	3.25-4.5	0.48-0.58	0.35-0.5	≤0.35	≤0.04	≤0.03	Bal.

The isothermal compression test of 21-4N was conducted under the deformation temperatures of 1273, 1333, 1393, and 1453 K, the strain rates of 0.01, 0.1, 1, 10 s^{-1} and the strain of 60% (the true strain was 0.916) by Gleeble-1500D simulator. The compressed model size is ø8×15 mm (As shown in Fig. 1 (a)). The deformation temperature was measured by thermocouple, and the date was collected by computer. Graphite lubricated sheets were attached to both ends of the sample to reduce frictional resistance. Fig. 1(b) shows the test process: the sample was heated to the set temperature at 10 K/s and holding 3 minutes. Then the sample is isothermal compressed at a constant strain rate. After that, water quenching immediately [14].

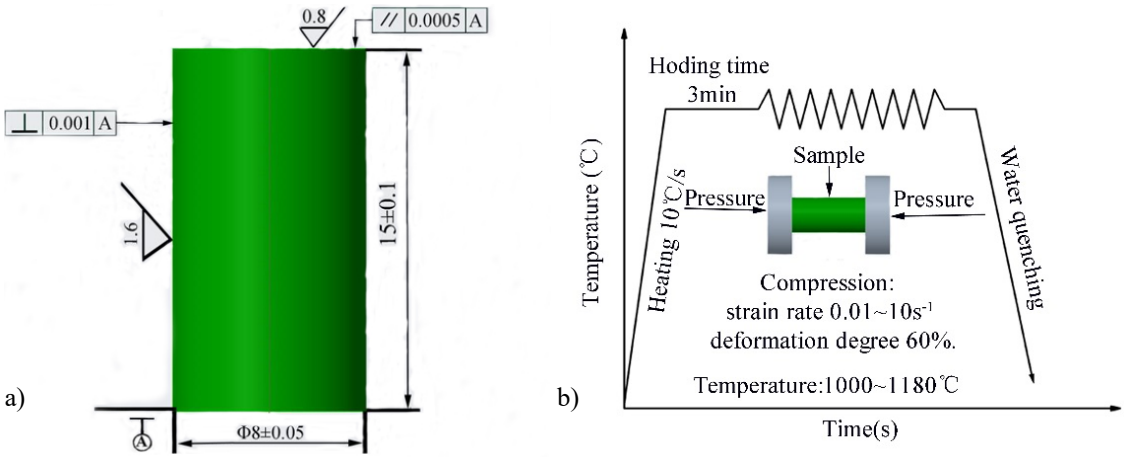

Fig. 1. (a) The size of compressed sample; (b) Test process

3. Results and Discussion

3.1. Flow Stress-Strain Behavior

The $\sigma - \varepsilon$ curves of 21-4N under different conditions was shown Fig. 2. And Fig. 2 shows the influences of the deformation conditions on flow stress. During deformation: dynamic recovery is the main softening mechanism at low-temperature and high-strain rate and DRX is the main softening mechanism at high-temperature and low-strain rate. High-temperature and low-strain rate make the flow stress decreases. The peak stress reaches minimum at 1453 K and 0.01 s^{-1}. Low-temperature and high-strain rate make the peak strain increases.

3.2. DRX Critical Strain Model and Peak Strain Model

3.2.1. Critical Strain Analysis Based on Work Hardening Rate

DRX refers to the phenomenon of recrystallization of metals during thermal deformation. The critical strain (ε_c) of DRX is an important indicator for studying the DRX of metals. The $\sigma - \varepsilon$ curves cannot directly reflect the critical strain when DRX occurs. Therefore, in order to determine the specific location where DRX occurs, it is necessary to further process the $\sigma - \varepsilon$ curves. Ryan et al. [16] firstly proposed the concept of work hardening rate ($\theta = \frac{d\sigma}{d\varepsilon}$), pointing out that the inflection point of $\theta - \sigma$ curve is the critical condition (Critical strain (ε_c)). The equation is as follow:

$$\frac{\partial}{\partial\sigma}\left(\frac{\partial\theta}{\partial\sigma}\right) = 0 \tag{1}$$

In the Eq. (1): θ – Work hardening rate, MPa; σ – Flow stress, MPa.

However, the $\theta - \varepsilon$ curves will amplify the experimental error in the fitting process, the position of the inflection point cannot be determined accurately. Therefore, Poliak et al. [17]

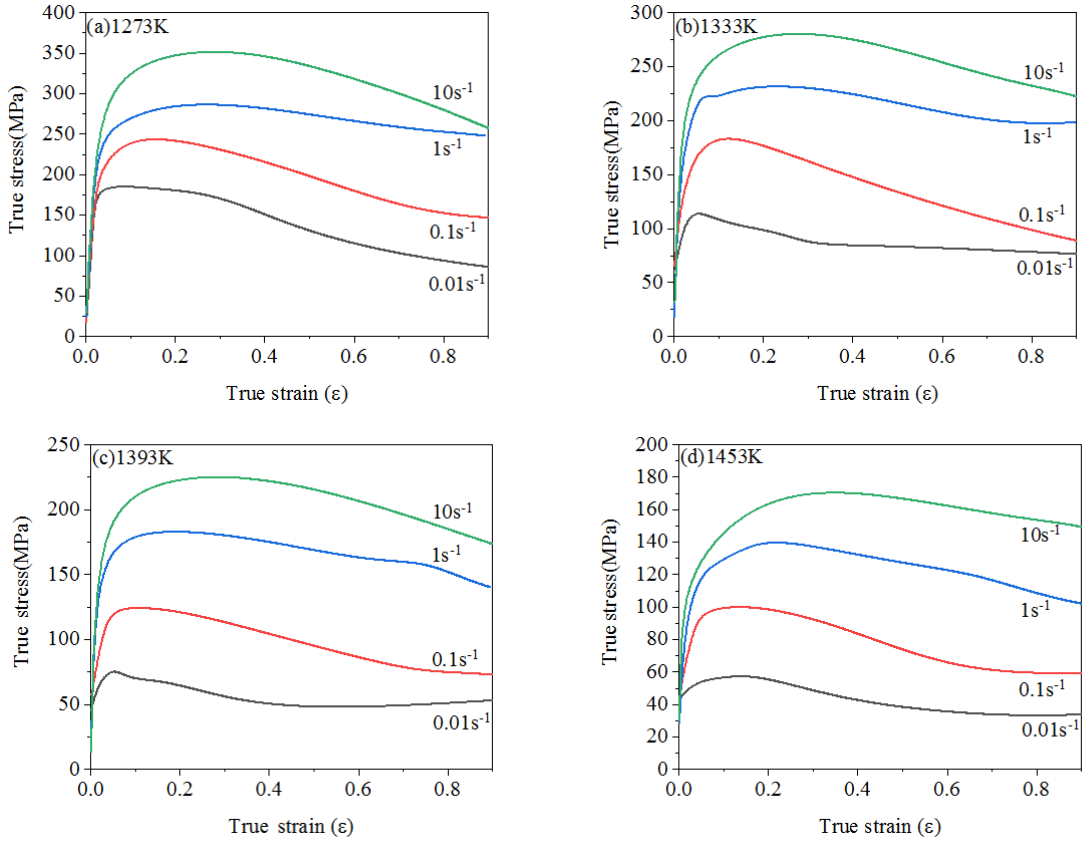

Fig. 2. $\sigma - \varepsilon$ curves of 21-4N at different strains with temperature of (a) 1273K; (b) 1333K; (c) 1393K; (d) 1453K [15]

and Ouyang et al. [18] proposed to calculate the inflection point of the $\theta - \sigma$ curves by using partial derivative. This method can reduce error that generated during the fitting process and obtain more accurate critical strains. The derivation process is as follow:

$$\frac{\partial\theta}{\partial\sigma} = \frac{\partial\theta}{\partial\varepsilon}\cdot\frac{\partial\varepsilon}{\partial\sigma} = \frac{1}{\theta}\cdot\frac{\partial\theta}{\partial\varepsilon} = \frac{\partial(\ln\theta)}{\partial\varepsilon} \tag{2}$$

In this paper, taking the conditions of 1333 K and 1 s^{-1} as an example to solve the critical strain. The Eq. (3) was used to fit the $\sigma - \varepsilon$ curves, and the fitting result was shown as Fig. 3.

$$\sigma = \frac{a_0 + a_1\varepsilon + a_2\varepsilon^2 + a_3\varepsilon^3 + a_4\varepsilon^4 + a_5\varepsilon^5}{b_0 + b_1\varepsilon + b_2\varepsilon^2 + b_3\varepsilon^3 + b_4\varepsilon^4 + b_5\varepsilon^5 + b_6\varepsilon^6} \tag{3}$$

Combining Eq. (2) with Eq. (3) to obtain $\ln\theta - \varepsilon$ and $-\frac{\partial(\ln\theta)}{\partial\varepsilon} - \varepsilon$. As shown in Fig 4, the critical strain under this condition can be obtained as 0.0786.

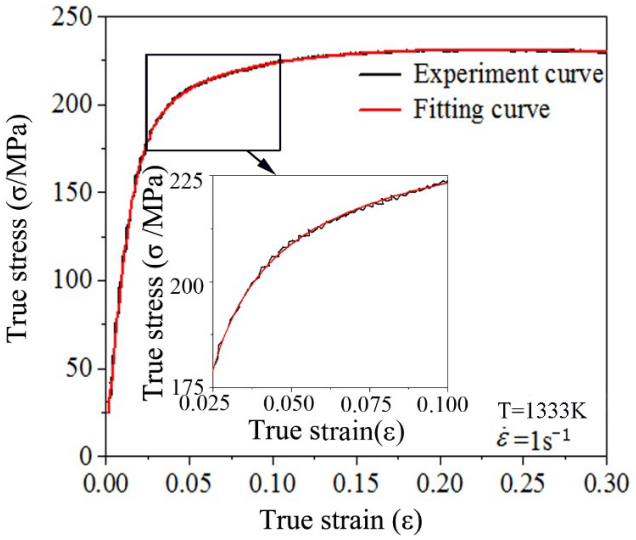

Fig. 3. $\sigma - \varepsilon$ measured curve and fitting curve with deformation temperature of 1333K and strain rate of 1s^{-1}

3.2.2. Critical Strain Model

By the same method as above, the ε_c under the temperatures of 1273, 1333, 1393, 1453 K, and strain rates of 0.01, 0.1, 1, 10 s^{-1} were calculated, respectively.

Fig. 5 is a three-dimensional line frame surface diagram. It shows the influence of different conditions on critical strain (ε_c) and peak strain (ε_p). From Fig. 5: when strain rate is constant, the influence of temperature on ε_c and ε_p is firstly negative and then positive. That is, ε_c and ε_p decrease firstly and then increase with the increasing of temperature. That is because as the temperature increases, the atomic thermal oscillation and diffusion rate also increase, the driving force of dislocation migration increases, and the critical shear stress of the slip system decreases, which is more conducive to the occurrence of DRX. When the temperature continues to increase and beyond certain

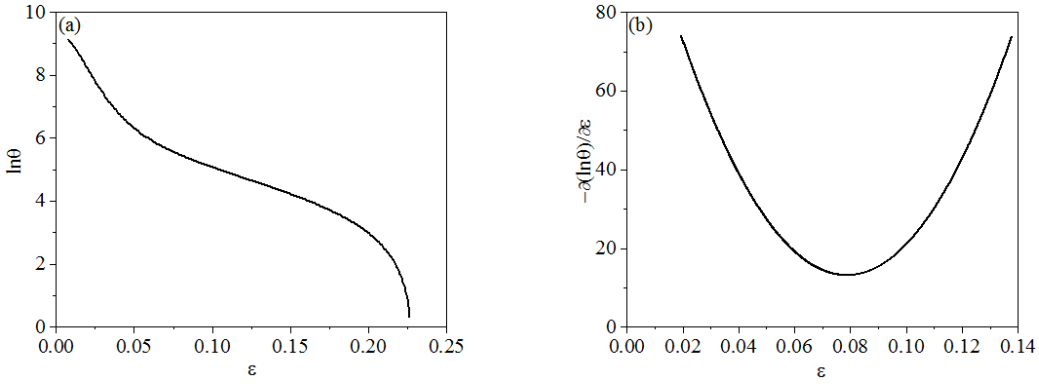

Fig. 4. The relationship between: (a) $\ln\theta$ and ε; (b) $-\partial(\ln\theta)/\partial\varepsilon$ and ε

range, DRX will cause softening, but then new work hardening will occur, which leads ε_c and ε_p to increase [19-20]. When the deformation temperature is constant, the influence of the strain rate on ε_c and ε_p strain is positive, that is ε_c and ε_p increase as the strain rate increases. That is because as the strain rate increases, the critical conditions also increase, the time for the combination of dislocations is reduced, and the recrystallized grains do not have sufficient time to nucleate and grow, which resulting in slow development of DRX [21].

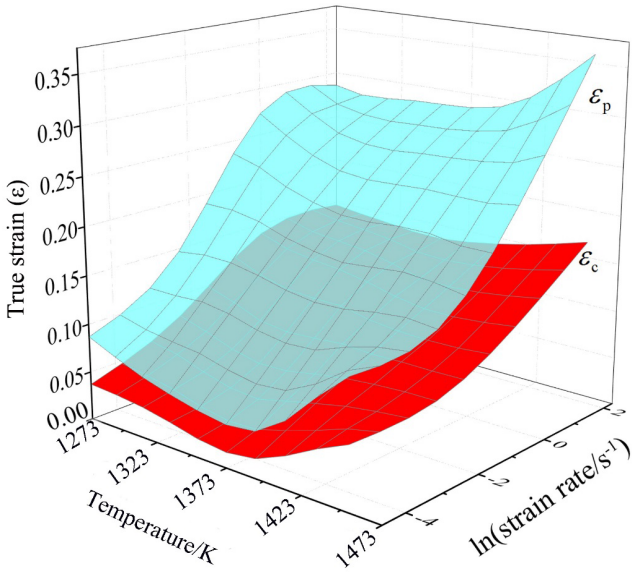

Fig. 5. Influence of deformation temperature and strain rate on ε_p and ε_c

In order to analyze the influence of the deformation conditions on ε_c more accurately, this paper adopted Sellars [22-23] model structure to characterize the critical strain model, as shown in Eq. (4):

$$\varepsilon_c = aZ^b \tag{4}$$

In the equation: a, b – Constant; Z – Temperature compensated strain rate factor, $Z = \dot{\varepsilon} \cdot \exp[Q/(RT)]$; R – Air constant, $8.3145 \cdot \text{mol}^{-1} \cdot \text{K}^{-1}$.

The parameters in Eq. (4) can be obtained by $Z = \dot{\varepsilon} \cdot \exp[Q/(RT)]$ and ε_c, as shown in Fig. 6.

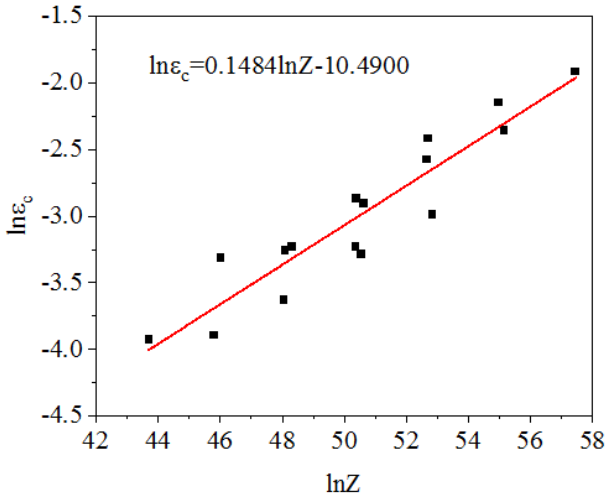

Fig. 6. The relationship between $\ln\varepsilon_c$ and $\ln Z$

3.2.3. Peak Strain Model

The relationship between ε_c and ε_p is shown in Fig. 7. From Fig. 7, ε_c is approximately linear with ε_p. Combining with Eq. (4), the predicted model of peak strain was obtained (Eq. 5).

$$\varepsilon_p = 1.74\varepsilon_c = 4.84 \times 10^{-5} Z^{0.1484} \tag{5}$$

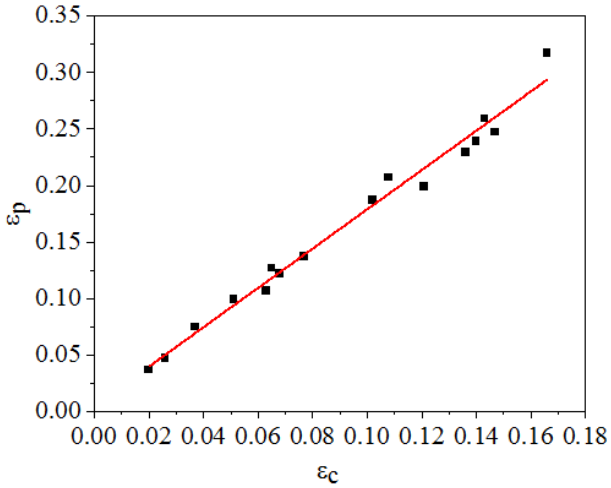

Fig. 7. The relationship between ε_p and ε_c

3.3. Volume Fraction Model

According to the dynamic theory of Jmak [24-26], the relationship between DRX volume fraction and deformation process parameters can be expressed by the Avrami equation (Eq. 6) [27].

$$X = 1 - \exp\left[-k\left(\frac{\varepsilon - \varepsilon_c}{\varepsilon_p}\right)^m\right] \quad (\varepsilon > \varepsilon_c) \tag{6}$$

In the Eq. (6): X – DRX volume fraction, %; k, m – Material parameters; ε – Strain; ε_p – Peak strain.

In general, the DRX volume fraction can be expressed by Eq. (7).

$$X = \frac{\sigma_{sat} - \sigma}{\sigma_{sat} - \sigma_{ss}} \tag{7}$$

In the Eq. (7): σ_{sat} – Dynamic recovery stress, it can be substituted in the calculation, MPa; σ_{ss} – Test steady stress, MPa; σ – Thermal deformation transient stress, MPa.

By calculation, m and k can be obtained, as shown in Table 2.

TABLE 2

The valves of m and k under different deformation conditions

Parameter	$\dot{\varepsilon}$/s^{-1}			
	0.01	**0.1**	**1**	**10**
m	1.215	2.149	3.122	2.009
k	0.1490	0.0774	0.1004	0.2254

Therefore, the DRX volume fraction kinetic models of 21-4N under different deformation conditions were obtained (Eq. (8)).

$$X = \begin{cases} 1 - \exp\left[-0.1490\left(\dfrac{\varepsilon - \varepsilon_c}{\varepsilon_p}\right)^{1.215}\right] & (\dot{\varepsilon} = 0.01) \\ 1 - \exp\left[-0.0774\left(\dfrac{\varepsilon - \varepsilon_c}{\varepsilon_p}\right)^{2.149}\right] & (\dot{\varepsilon} = 0.1) \\ 1 - \exp\left[-0.1004\left(\dfrac{\varepsilon - \varepsilon_c}{\varepsilon_p}\right)^{3.122}\right] & (\dot{\varepsilon} = 1) \\ 1 - \exp\left[-0.2254\left(\dfrac{\varepsilon - \varepsilon_c}{\varepsilon_p}\right)^{2.009}\right] & (\dot{\varepsilon} = 10) \end{cases} (\varepsilon > \varepsilon_c) \tag{8}$$

3.4. Grain Size Model

The DRX grain size refers to the grain size when the metal or alloy reaches the steady state during the DRX process. When the deformation enters the steady state, the DRX grain size remains basically unchanged with the increase of the strain. And there is a certain functional relationship between grain size and Zener-Holloman (Eq. (9)).

$$d_{drx} = C Z^a \tag{9}$$

In the equation: C, a – Material parameters.

Quantitative test of grain size of samples was subjected to DRX on the Image Pro Plus 6.0 by using the cutting line method, the results are shown in Table 3. By calculating, C and a can be obtained, and the DRX grain size models also obtained, as shown in Eq. (10).

$$d_{drx} = \begin{Bmatrix} 9.11\times10^2 Z^{-0.1006} & (\dot{\varepsilon} = 0.1) \\ 2.05\times10^3 Z^{-0.1098} & (\dot{\varepsilon} = 1.0) \\ 7.67\times10^3 Z^{-0.1272} & (\dot{\varepsilon} = 10) \end{Bmatrix} \tag{10}$$

TABLE 3

Grain size under different deformation conditions

$\dot{\varepsilon}$/s^{-1}	T/K	ln$Z$	lnd_{drx}
0.1	1273	52.849	1.509
	1333	50.366	1.725
	1393	48.098	1.988
1	1273	55.151	1.562
	1333	52.669	1.858
	1393	50.400	2.083
10	1273	57.454	1.607
	1333	54.972	2.024
	1393	52.703	2.208

3.5. Model Accuracy Verification

This paper introduced the average relative error (AARE) and correlation coefficient (RR) to verify the accuracy of models, as shown in Eq. (11), Eq. (12). The smaller the AARE is and the closer the RR is to 1, the higher the accuracy of the model.

$$AARE(\%) = \frac{1}{N}\sum_{i=1}^{N}\left|\frac{E_i - P_i}{E_i}\right| \times 100\% \tag{11}$$

$$RR = \frac{\sum_{i=1}^{N}\left(E_i - \bar{E}\right)\left(P_i - \bar{P}\right)}{\sqrt{\sum_{i=1}^{N}\left(E_i - \bar{E}\right)^2\left(P_i - \bar{P}\right)^2}} \tag{12}$$

In the equation: E – Experimental value; P – Predicted value (calculated value); $\bar{E}, \bar{P}$ – Average of experimental and predicted values.

The AARE and RR of four models were obtained by using Eq. (11) and Eq. (12), as shown in Table 4. And Fig. 8 shows the correlation between experimental and predicted values of four models.

TABLE 4

The AARE and RR of four models

Types of model	Critical Strain	Peak Strain	DRX Volume Fraction	Grain Size
AARE/%	9.0113	9.0962	10.3877	2.3288
RR	0.95435	0.98967	0.99487	0.98983

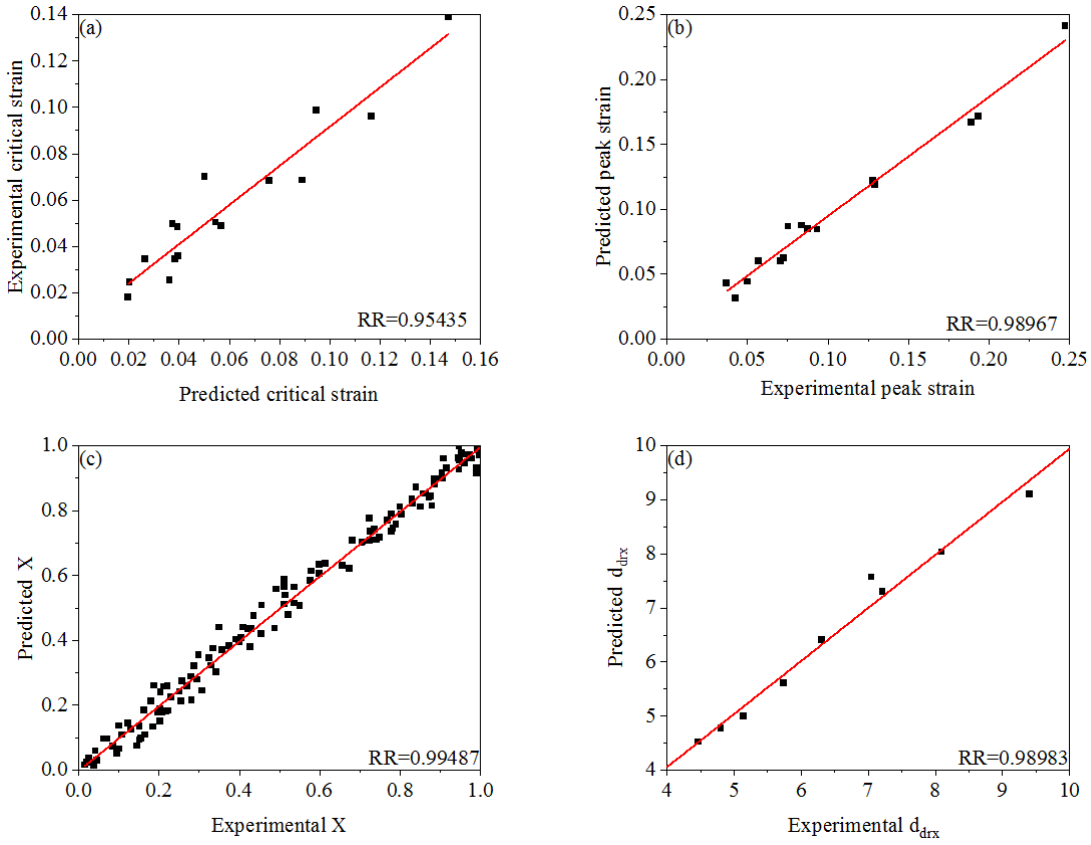

Fig. 8. The correlation between experimental grain sizes and predicted of four models: (a) critical strain; (b) peak strain; (c) volume fraction; (d) grain size

In summary, the AARE of each model and the RR of the fitted curves are within a reasonable range, indicating that the established models can well describe the DRX process of 21-4N during hot deformation.

3.6. Microstructure Observation

Whether metals and alloys undergo DRX is mainly determined by deformation degree, strain rate, deformation temperature and the nature of the material itself [28-30]. Under the precondition of metal material and processing technology, the DRX of material is greatly affected by deformation degree. Under the same deformation conditions, when the strain of the material increase, the internal storage energy and the driving force of the DRX increase correspondingly, which makes the rate increases and the temperatures decrease.

In this paper, Image-Pro Plus 6.0 software (IPP) was used to measure the grain size of microstructure of 21-4N heat-resistant steel by transversal method. Transversal method is one of the common methods to measure grain size of metal and alloy microstructure. The specific method is as follow: Intercepting the grain with a random line, if the total length of the measured line is L_T and the number of truncated grains is N, the average transversal length of continuous distributed single-phase austenite grains is $L_3 = L_T/N$. L_3 is the transversal length of a 3D object. It refers to the average transversal length in the object when a 3D object is randomly intercepted. When the number of measurements is sufficient, the length of the 2D section $L_2 = L_3$.

Fig. 9 shows the original microstructure of 21-4N (Fig. 9(a)) and the microstructure under the conditions of the temperature is 1333K and the strain rate is $10s^{-1}$. From Fig. 9(a), the original microstructure of the 21-4N is basically composed of equiaxed grains whose size is about 11.4 μm. From the remaining three figures, the DRX fraction increases as the strain increases. When the strain is 20%, DRX does not occur substantially, and only a few of fine crystal grains are formed around the grain boundary, which indicates that the grain boundary is a favorable position for DRX nucleation. As the strain increases, the storage energy inside the metal can be further improved, the driving force of DRX increases, making the DRX fraction increases gradually, and the newly generated DRX grains are irregularly arranged along the grain boundary (Fig. 9(c) and (d)). With the strain increasing, the DRX grains and fraction also increase. When the strain reached 60%, DRX completed substantially, the average valve of the grain size is 5.7 μm.

4. Conclusion

1) The peak stress of 21-4N increases with the decrease of deformation temperature and increase of strain rate. The DRX of 21-4N is remarkable at higher deformation temperature and lower strain rate. Work hardening causes the flow stress

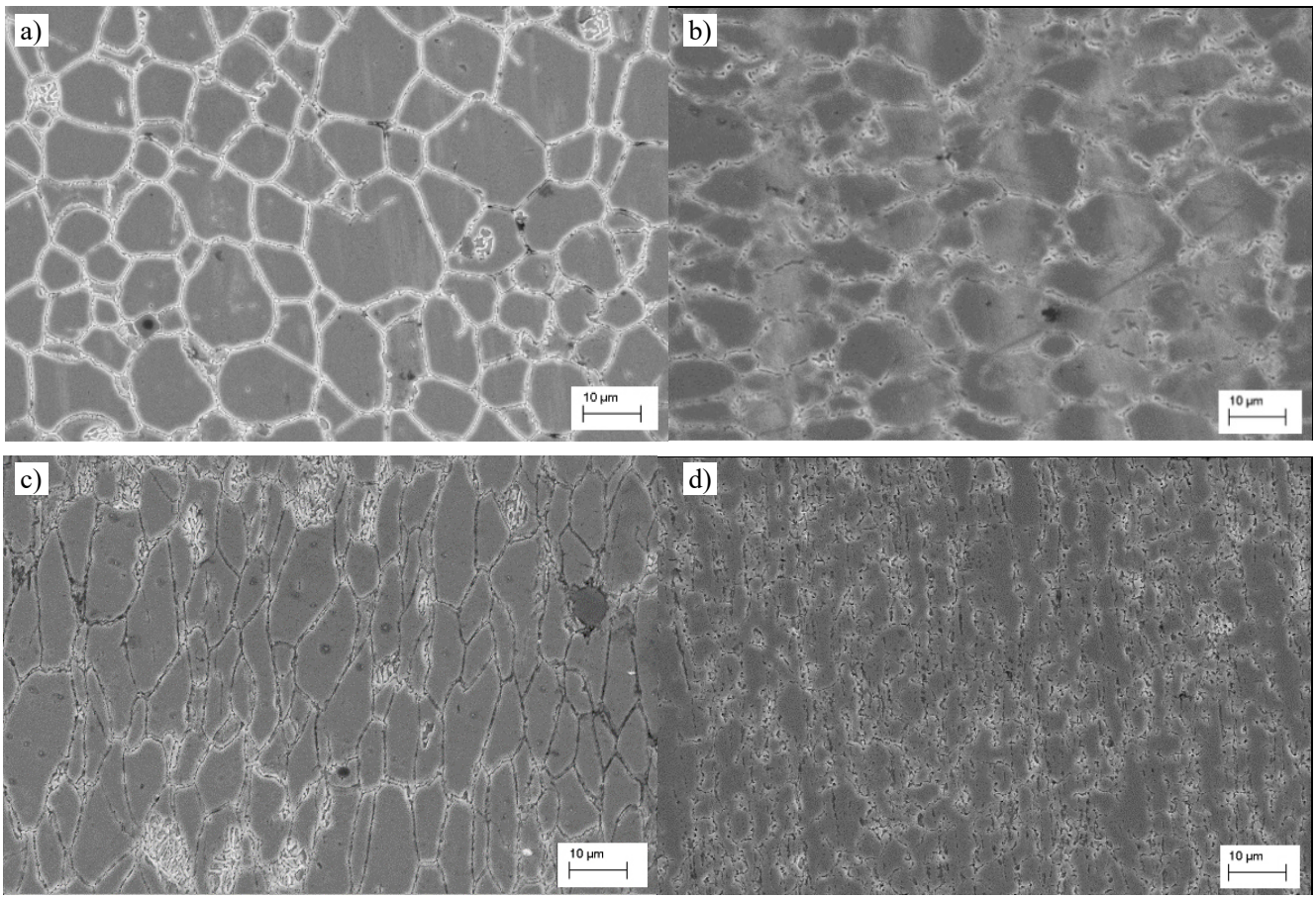

Fig. 9. Microstructure under different deformation degree: (a) Original microstructure; (b) $T = 1333$K, $\dot{\varepsilon} = 10s^{-1}$, $\varepsilon = 20\%$; (c) $T = 1333$K, $\dot{\varepsilon} = 10s^{-1}$, $\varepsilon = 40\%$; (d) $T = 1333$K, $\dot{\varepsilon} = 10s^{-1}$, $\varepsilon = 60\%$

to reach peak valve quickly, then drops to a stable value slowly and enters a stable deformation stage.

2) According to the results of thermal compression simulation and quantitative metallographic experiments, the work hardening rate-strain curves are drawn. The critical strains of DRX of 21-4N are determined. The DRX critical strain model and peak strain model of 21-4N are established.
3) The DRX volume fraction models and grain size models of 21-4N are established by Avrami equation.
4) The microstructures of 21-4N are observed, which are consistent with the calculated results.

Acknowledgements

This work is supported by the China Postdoctoral Science Foundation (Grant No. 2018M641186).

REFERENCE

[1] M.E. Mehtedi, P. Ricci, L. Drudi, S.E. Mohtadi, M. Cabibbo, S. Spigarelli, Mater. Design. **33**, 136-144 (2012).
[2] H.C. Ji, J.P. Liu, B.Y. Wang, X.F. Tang, J.G. Lin, Y.M. Huo, J. Alloy Compd. **693**, 674-687 (2017).
[3] R.D. Doherty, D.A. Hughes, F.J. Humphreys, J.J. Jonas, J.D. Juul, M.E. Kassner, W.E. King, T.R. Mcnelley, H.J. Mcqueen, A.D. Rollett, Mat. Sci. Eng. A. **238**, 219-274 (1997).
[4] R.W.K. Honeycombe, R.W. Pethen, J. Less-Com. Metals. **28** (2), 201-212 (1972).
[5] S.L. Wang, M.X. Zhang, H.C. Wu, B. Yang, Mater. Charact. **118**, 92-101 (2016).
[6] J. Favre, D. Fabregue, K. Yamanaka, A. Chiba, Mat. Sci. Eng. A. **653**, 84-92 (2016).
[7] B. Fang, Z. Ji, M. Liu, G.F. Tian, C.C. Jia, T.T. Zeng, B.F. Hu, Y.H. Chang, Mat. Sci. Eng. A. **593**, 8-15 (2014).
[8] J. Liu, Z. Cui, L. Ruan, Mat. Sci. Eng. A. **529**, 300-310 (2011).
[9] H. Jiang, L. Yang, J.X. Dong, M.C. Zhang, Z.H. Yao, Mater. Design. **104**, 162-173 (2016).
[10] G. Ji, Q. Li, L. Li, Mat. Sci. Eng. A. **586**, 197-203 (2013).
[11] Y. Xu, L. Hu, Y. Sun, J. Alloy Compd. **580**, 262-269 (2013).
[12] T.J. Baron, K. Khlopkov, T. Pretorius, D. Balzani, Steel Res. Int. **87**, 37-45 (2016).
[13] M.S. Chen, Y.C. Lin, X.S. Ma, Mat. Sci. Eng. A. **556**, 260-266 (2012).
[14] Y.M. Li, H.C. Ji, W.D. Li, Y.G. Li, W.C. Pei, J.P. Liu, Materials. **12**, 89-107 (2019).
[15] H.C. Ji, X.M. Huang, C.J. Ma, W.C. Pei, J.P. Liu, B.Y. Wang, Metals. **8**, 391-409 (2018).
[16] N.D. Ryan, H.J. Mcqueen, J. Mater. Process. Tech. **21**, 177-199 (1990).

[17] E.I. Poliak, J.J. Jonas, Acta. Mater. **44**, 127-136 (1996).
[18] D.L. Ouyang, S.Q. Lu, X. Cui, K.L. Wang, C. Wu, Rare Metal Mat. Eng. **40** (2), 325-330 (2011).
[19] C.Y. Sun, J.D. Luan, G. Liu, R. Li, Q.D. Zhang, Acta. Metall. Sin. **48**, 853-860 (2012).
[20] L. Ren, J. Wu, G. Quan, Mat. Sci. Eng. A. **612**, 278-286 (2014).
[11] G.Z. Quan, Y. Shi, Y.X. Wang, B.S. Kang, T.W. Ku, W.J. Song, Mat. Sci. Eng. A. **528**, 8051-8059 (2011).
[22] C.M. Sellars, Metal Sci. **1** (4), 325-332 (2013).
[23] C.M. Sellars, J A Whiteman, Metal Sci. **13**,187-194 (1979).
[24] Rios, R. Paulo, E. Villa, Mater. Sci. Forum. **753**, 137-142 (2013).
[25] M.C. Weinberg, D.P.B. Iii, V.A. Shneidman, J. Non-Cryst. Solids. **219**, 89-99 (1997).
[26] P. Honarmandi, M. Aghaie-Khafri, Metall. Mic. Analysis. **2**, 13-20 (2013).
[27] V. Sencadas, C.M. Costa, J.L. Gómez-Ribelles, S. Lanceros-Mendez, J. Mater. Sci. **45**, 1328-1335 (2010).
[28] X.M. Chen, Y.C. Lin, D.X. Wen, J.L. Zhang, M. He, Mater. Design. **57**, 568-577 (2014).
[29] Y.C. Lin, X.M. Chen, Mater. Design. **32**, 1733-1759 (2011).
[30] Y.C. Lin, M.S. Chen, J. Zhong, T. Mater. Heat Treat. **1**, 70-74 (2009).